NASA/TP—2000–210386

The Use of Ferrofluids to Model Materials Processing

(MSFC Center Director's Discretionary Fund Final Report, Project No. 98–12)

F. Leslie
Marshall Space Flight Center, Marshall Space Flight Center, Alabama

N. Ramachandran
Universities Space Research Association, Huntsville, Alabama

National Aeronautics and
Space Administration

Marshall Space Flight Center • MSFC, Alabama 35812

July 2000

Acknowledgments

This work was supported by funding from NASA MSFC Center Director Discretionary Fund. The work by N. Ramachandran was done under the auspices of the Alliance for Microgravity Materials Science and Applications through NASA contract NCC8-66. The authors would also like to acknowledge Mr. Charles Sisk for his efforts in measuring the magnetic field and Soyoung Cha for his assistance with the camera calibration.

Trademarks

Available from:

NASA Center for AeroSpace Information
7121 Standard Drive
Hanover, MD 21076–1320
(301) 621–0390

National Technical Information Service
5285 Port Royal Road
Springfield, VA 22161
(703) 487–4650

TABLE OF CONTENTS

LIST OF FIGURES

LIST OF TABLES

ABBREVIATIONS AND SYMBOLS

$\alpha_1(x,y)$	attentuation coefficient of first wall
$\alpha_2(x,y)$	attentuation coefficient at second wall
α_λ	extinction coefficient of the ferrofluid
β	density coefficient
δ	diameter of magnetic particles
μ_o	permeability of free space
ν	kinematic viscosity
ρ	fluid density
ρ_o	density at ϕ=0
ϕ	volume fraction of solid magnetic particles
a	test cell width
b	test cell depth
C	concentration
C_K	known constant fluid concentration
C_{mo}	initial concentration in the mixer
C_r	concentration in the supply syringe
C_v	volume concentration of the ferrofluid
$\mathbf{g}$	gravity
H	strength of the applied magnetic field
$I_o(x,y)$	initial (non-uniform) intensity
$I_D(x,y)$	image intensity at D
I_D^K	digital array of known concentration
k	Boltzmann's constant
M	magnetization of the fluid

M_d	magnetization of the bulk magnetic solid
M_s	maximum (saturation) magnetization
p	pressure
T	absolute temperature
$\mathbf{V}$	velocity
v_{final}	final volume of fluid in the test cell
v_m	volume of the mixer
v_{mo}	initial volume of the mixer
v_{ro}	initial reservoir volume
v_t	total volume deployed

TECHNICAL PUBLICATION

THE USE OF FERROFLUIDS TO MODEL MATERIALS PROCESSING
(MSFC Center Director's Discretionary Fund Final Report, Project No. 98–12)

1. INTRODUCTION

A great number of crystals grown in space are plagued by convective motions, which contribute to structural flaws. The character of these instabilities is not well understood but is associated with density variations in the presence of residual gravity and g-jitter. As a specific example, past mercury cadmium tellurium (HgCdTe) crystal growth space experiments by Gilies et al.[1] indicate radial compositional asymmetry in the grown crystals. In the case of HgCdTe, the rejected component into the melt upon solidification is mercury tellurium (HgTe) which is denser than the melt. The space-grown crystals indicate the presence of three-dimensional flow with the heavier HgTe-rich material clearly aligned with the residual gravity (0.55–1.55 μg) vector. This flow stems from multicomponent convection, namely, thermal and solutal buoyancy-driven flow in the melt. A model, fluids experiment to study this problem in space requires the rapid development of a concentration (density) gradient which is difficult to establish in the absence of a stabilizing gravitational field. An important objective of this study is to evaluate the feasibility of using a magnetic fluid to study this phenomenon. Once the effectiveness of a magnetic field in stabilizing the concentration gradient is established, the developed techniques can be utilized in the design of a space experiment to study the crystal growth instability problem.

When a magnetic or ferrofluid is placed in an appropriate magnetic field, the induced body force can be utilized for fluid manipulation. This technique is also significant in its potential for greatly improving the performance and lowering the cost of spacecraft thermal management systems. For example, terrestrial electronic systems often rely on gravity driven natural convection for heat rejection. In the reduced gravity environment of space, (i.e., Earth orbit, Moon, Mars), natural convection heat-transfer rates are so diminished that innovative solutions are required to efficiently reject heat and maintain the system at an acceptable temperature. The ease of essentially dialing in the required body force (gravity level) holds the promise of active thermal control (dynamically enhancing or suppressing convective heat transfer rates) of space systems.

Artificial ferrofluids are typically colloidal suspensions of extremely small ferrite particles that have been treated with a surfactant to prevent clumping and settling, (see Odenbach[2] for experiments allowing for the demixing of the magnetic particles and the resulting forced diffusion that drives convection). Although a multiphase mixture at the microscopic scale, the nearly uniform dispersion of very small particles permits ferrofluids to be well represented by a continuum model. Neuringer and Rosensweig[3] present the fundamental hydrodynamic equations describing the flow of a ferrofluid and highlight the primary phenomena arising from the coupling between an imposed magnetic field and the fluid flow.

Most applications of ferrofluids involve their use in very small-scale devices or as a thin film that is subjected to magnetic, gravitational, and heating effects. Highly successful applications of this technology include printers, pumps, clutches, brakes, and seals. Driven by these applications, research has focused on interfacial stability limits, magnetization effects on buoyancy and thermocapillary convection, fluid flow in simple planar or cylindrical geometries, and the deformation of simple surfaces and drops. Zelazo and Melcher[4] studied the dynamics and stability of ferrofluids with particular emphasis on surface interactions. They found that, although the nonlinear magnetization characteristics of ferrofluids complicate wave dynamics and stability, the magnetic coupling with homogeneous fluids is confined to interfaces. They also noted that the magnetic force can provide a stabilizing effect on a Rayleigh-Taylor instability. Finlayson[5] studied the convective instability of a ferrofluid layer heated from below in the presence of a uniform vertical magnetic field and found that the magnetic field can suppress buoyant convection. Bashtovoi, and Krakov[6] and Bashtovoi[7] examined the stability of magnetizable liquid layers and jets in the presence of uniform magnetic fields. They showed that the magnetic forces lead to nonuniform pressure distributions, which can have a significant effect on the stability of the flow. Bashtovoi[8] also studied the problem of magnetic convection of a ferrofluid heated from below and found the problem similar to the classic Rayleigh instability of a classical fluid in the presence of a gravitational field alone. The additional magnetic body force resulted in a more comprehensive Rayleigh number containing magnetic properties that predicts the onset of convection. The magnetic Rayleigh-Bérnard problem was also studied by Schwab et al.[9] and by Stiles and Kagan.[10] One of the few studies involving non-equilibrium magnetization was performed by Rosensweig et al.[11] who examined the flow of a ferrofluid in a rotating magnetic field.

Nakatsuka et al.[12] performed experiments to study the heat-transfer rate of a simple heat siphon in a magnetic field. Their data show that the heat-transfer rate of a vertical wire in a magnetic fluid can be enhanced with the application of a magnetic field. Aihara et al.[13] numerically modeled the convection of a magnetic fluid flowing through a circular tube with an axial magnetic field. They showed that as the Reynolds number of the flow decreased, the magnetic force becomes more effective in transporting the heat. More recently, Zebib[14] examined theoretically an internally heated cylindrical shell with a radial magnetic field acting on a ferrofluid fluid. His calculations determined the critical magnetic Rayleigh number for the onset of convection in this geometry within the constraints of his model. The convection took the form of a number of counter-rotating rolls in the radial azimuthal plane transferring heat from the inner cylinder to the outer wall.

The study of naturally occurring paramagnetic and diamagnetic fluids has not been as extensive as the study of ferrofluids because their magnetization is so weak that forces induced by the presence of a magnetic field are usually negligible with respect to gravitational forces. Notable exceptions are liquid coolant lines in plasma confinement systems and particle accelerators where exceptionally strong magnetic fields occur. Berkovsky and Smirnov[15] developed a theoretical framework for mathematically modeling these flows which utilizes the same basic equations and boundary conditions that were developed for the ferrofluid studies.

There have been very few experiments with magnetic heat transport in a reduced gravity environment. Hörsten et al.[16] flew an experiment in a TEXUS sounding rocket that examined the convection of a magnetic fluid inside a cylindrical shell with gradients of the temperature and magnetic fields in the radial direction. Results showed radial-azimuthal convection cells as anticipated, although only two appeared

instead of the expected eight. Odenbach[17] also conducted experiments in low-gravity using a drop tower. In spite of the short duration of low gravity, his experiments showed a critical magnetic Rayleigh number of 1820±100 needed for the onset of magnetic convection in a cylindrical shell. Odenbach[18], repeating the experiments using a sounding rocket, obtained similar results.

In summary, although the effect of a magnetic field on the flow of a ferrofluid or a paramagnetic fluid has been under study for >35 yr, understanding of this influence and its interaction with competing forces such as gravity and surface tension is still in its infancy. Understanding of the combined effect of all these forces on heat transfer is even less developed. The investigations have been primarily small-scale experiments in a normal gravity environment with the addition of a few recent experiments that used a reduced gravity environment to help expose the relationships between the competing influences.

The present study examines a technique that may be useful for studying instabilities which plague crystal growth experiments in space. In these experiments, there is an exponential distribution of species concentration in the region close to the crystal. When these density variations are acted upon by the residual gravity (g-jitter), flow instabilities develop which impact the growth process. To study these instabilities in a separate, controlled experiment, a concentration gradient would have to be artificially established in a timely manner as an initial condition. This is generally difficult to accomplish in a microgravity environment because the momentum of the fluid injected into a test cell tends to swirl around and mix. However, the use of a magnetic fluid would allow it to be held in position during deployment and then released by switching off the magnetic field before starting the experiment. The following describes a technique for such a deployment and measurement of the resulting concentration field.

2. THEORETICAL CONSIDERATIONS

For the isothermal liquid considered, two forces contribute to the distribution of the ferrofluid, namely the magnetic body force and gravity acting on density differences. In a ground-based laboratory, the magnetic gradient could certainly be positioned in the same direction as gravity to provide an assisting force for holding the gradient in place. However, in order to evaluate the effectiveness of the magnetic force and the response of the liquid, the field gradient was established opposite gravity. Consequently, it is important to ensure that the magnetic force can be made sufficiently strong to overcome the fluid density.

Rosensweig[19] showed that the governing equation for a magnetic fluid is

$$\rho \frac{d\mathbf{V}}{dt} = -\nabla \mathrm{p} + \rho \nu \nabla^2 \mathbf{V} + \rho \mathbf{g} + \mu_o M \nabla H \quad , \tag{1}$$

where ρ is the fluid density, $\mathbf{V}$ is the velocity, p is the pressure, ν is the kinematic viscosity, $\mathbf{g}$ is gravity, μ_o is the permeability of free space, M is the magnetization of the fluid, and H is the strength of the applied magnetic field. The last term of eq. (1) shows that a magnetic fluid can be driven toward the regions of higher magnetic field. Let us define the density coefficient β (after Turner[20]) at constant temperature T as:

$$\beta \equiv \frac{1}{\rho} \frac{d\rho}{d\phi}\Bigg)_T \quad , \tag{2}$$

where ϕ is the volume fraction of solid magnetic particles present (a measure of concentration). Thus,

$$\rho(\phi) = \rho_o + \frac{d\rho}{d\phi}\phi \ ,$$

where ρ_o is the density at ϕ=0.

Now eq. (1) becomes

$$\rho \frac{d\mathbf{V}}{dt} = -\nabla \mathrm{p} + \rho \nu \nabla^2 \mathbf{V} + \mathbf{g}\left(\rho_o + \frac{d\rho}{d\phi}\phi\right) + \mu_o M \nabla H \quad , \tag{3}$$

Substituting eq. (2) into eq. (3) yields

$$\rho\frac{d\mathbf{V}}{dt} = -\nabla \mathrm{p} + \rho\nu\nabla^2\mathrm{V} + \mathbf{g}(\rho_o + \rho\beta\phi) + \mu_o M\nabla H \ , \tag{4}$$

If we arbitrarily align the z-axis with gravity such that $\mathbf{g} = -g\hat{k}$ and similarly position the magnetic field in opposition such that $\nabla H = \frac{dH}{dz}\hat{k}$, then eq. (4) becomes

$$\frac{d\mathbf{V}}{dt} = -\frac{1}{\rho}\nabla \mathrm{p}^* + \nu\nabla^2\mathbf{V} + \hat{k}\left(\frac{\mu_o M}{\rho}\frac{dH}{dz} - \beta\phi g\right) \ , \tag{5}$$

where $\mathrm{p}^* = \mathrm{p} + \rho_o g z$.

It is clear from eq. (5) that for a magnetic field increasing upward, the last two terms compete for the distribution of the liquid, since regions of high particle concentration settle downward unless the magnetic field gradient is strong enough to compensate. More precisely, the magnetic effect can overcome gravity if

$$\frac{dH}{dz} > \frac{\rho\beta\phi g}{M\mu_o} \ . \tag{6}$$

The magnetization of the fluid, M, depends on the applied magnetic field. The ferrofluid consists of small magnetic particles of diameter δ that are randomly oriented by Brownian motion in the absence of an applied magnetic field, resulting in no net magnetization of the fluid. If an external field H is applied, the fluid becomes magnetized as the particles align somewhat when the field strength is greater than the energy of the Brownian motion, kT where k is Boltzmann's constant and T is absolute temperature. If the field is increased further, there is a greater degree of alignment of the particles and the fluid magnetization increases. At some large field value, all of the particles will align and the fluid reaches its maximum (or saturation) magnetization, M_s. This saturation value is given by $M_s = \phi M_d$, where ϕ is the volume fraction of solid particles in the fluid and M_d is the magnetization of bulk magnetic solid. The fluid magnetization is given by the Langevin formulation[19] as

$$\frac{M}{\phi M_d} = L(\xi) \ , \tag{7}$$

where $L(\xi) = \coth(\xi) - \frac{1}{\xi}$ and $\xi = \frac{\pi}{6}\frac{\mu_o M_d H \delta^3}{kT}$. Thus the requirement for dominance of the magnetic force in the fluid over gravity becomes

$$\frac{dH}{dz} > \frac{\rho \beta g}{M_d L(\xi) \mu_o} \quad . \tag{8}$$

Consequently, the necessary field gradient is independent of the volume fraction of solid particles. The ferrofluid used in this study (EMG 909 manufactured by Ferrofluidics Corporation of Nashua, NH) consists of 10-nm magnetite particles suspended in a light mineral oil carrier. These particles have a magnetization, M_d, of 4.46×10^5 A/m so that the fluid magnetization can be computed from eq. (7) and is shown in fig. 1. Note that for very large field values, the fluid magnetization approaches a saturation value of 201 G.

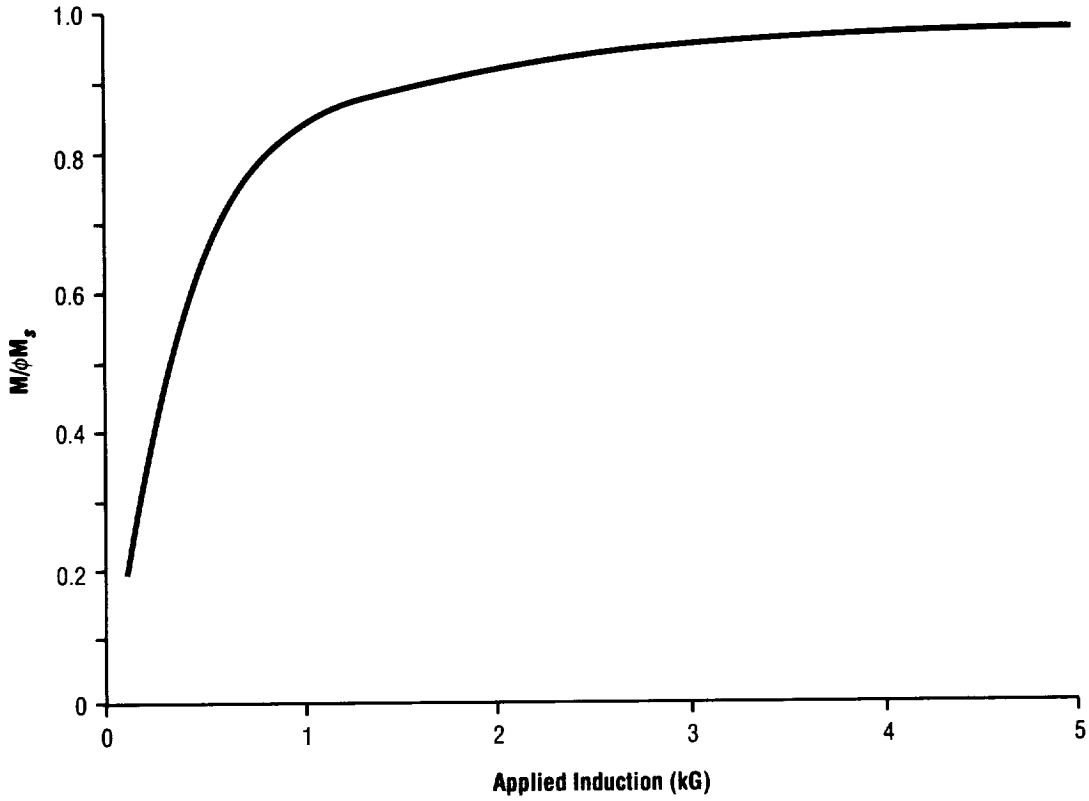

Figure 1. Magnetization curve of ferrofluid used in this study.

To evaluate $L(\xi)$, the magnetic field used in the experiment was mapped out in two dimensions using a three-dimensional Hall probe and is shown in fig. 2. The lower part of this field where the vertical gradient is uniform is the region where the experiments were conducted and $L(\xi)$ has a value of about 0.88 while the gradient is $\approx$100 G/cm. The value of $\rho\beta$ was measured to be $\approx$6,720 kg/m^3 (see app. A). With this information, the minimum field gradient necessary to overcome gravity is calculated to be 16.8 G/cm and thus eq. (8) is satisfied. In a space laboratory environment, this requirement would be particularly easy to achieve since the apparent gravity is so small. Consequently, even a very weak magnetic field would be adequate and fluids of low magnetization could also be employed.

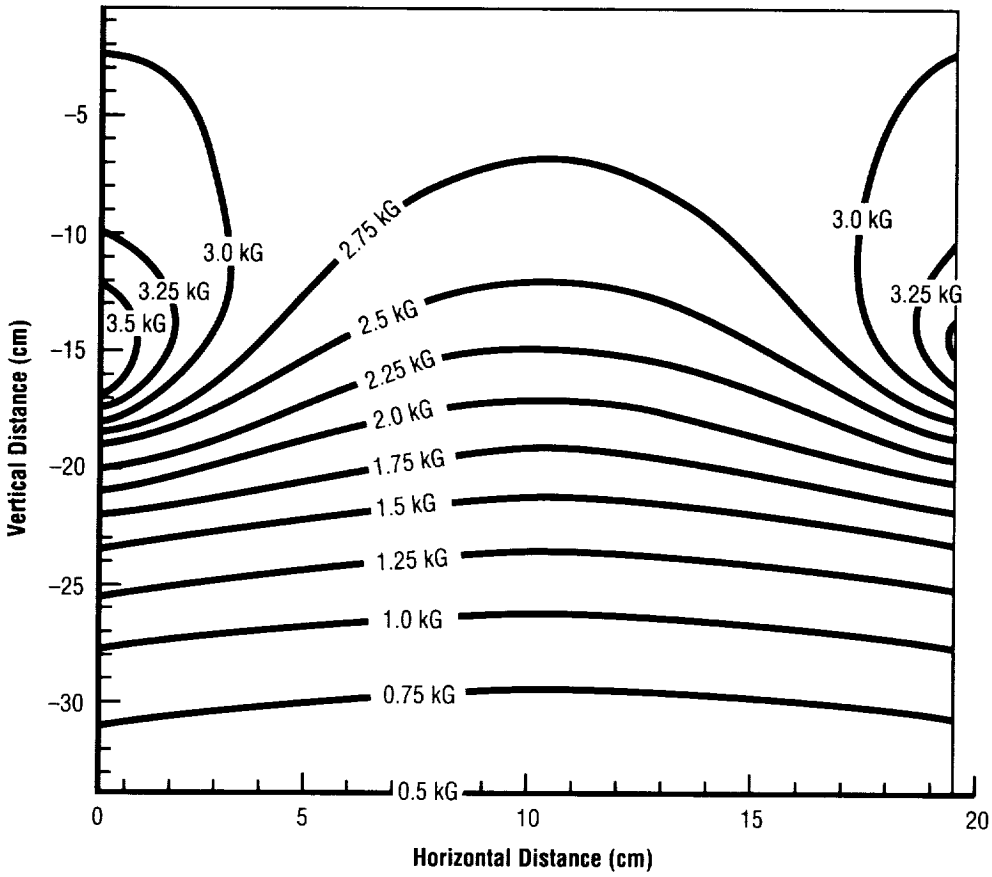

Figure 2. Measurements of the magnetic field in the vertical plane of the experiment.

3. EXPERIMENT CONFIGURATION

The primary objective of this effort is to develop a method for quickly producing an exponential gradient applicable to space experiments. By demonstrating this technique on the ground using a strong magnetic field to overcome gravity, we can be assured that this method would be relevant to space systems using a substantially weaker field.

A gradient former was used to produce the desired concentration distribution. It consists of a dual syringe system, with one syringe containing pure solvent and the other the solute solution. By deploying two liquids in different proportions into a mixing chamber and eventually into the test cell, precise gradients ranging from linear to exponential can be realized within minutes (see app. B). This mechanism works well in terrestrial laboratories where gravity assists in maintaining a stable stratification. In low gravity, however, there is no restoring force to prevent swirling of the fluid as it is introduced into a test cell. This jetting effect would immediately mix the liquid.

One way of stabilizing the required solute gradient is by using a magnetic fluid and a controlling magnetic field to provide the required body force in the gradient former arrangement. A practical implementation of an exponential gradient setup is shown in fig. 3. It consists of a supply syringe or reservoir (syringe 1) and a mixer. Syringe 2, shown in fig. 3, is used during the initial filling operations of the supply syringe and the mixer. The gradient former deploys into the test cell a solution of gradually decreasing concentration of the ferrofluid as the supply syringe is depressed. The magnetic field from the electromagnet provides the body force that interacts with the varying solution magnetism, much like gravity allows the setup of a solute gradient due to solution density variations. Because the ferrofluid is very opaque, it was diluted further with the mineral oil (carrier) to a concentration of 0.5 percent by volume (hereafter known as the test solution) to allow viewing of the concentration gradients with a camera and to facilitate non-intrusive optical diagnostics.

The test cell measures 10 mm wide by 10 mm deep by 40 mm high, and was positioned below the magnet. The mixer is initially filled with test solution while the supply syringe only contained the carrier. In this manner, the fluid entering the test cell has diminishing concentration. Tubing used to connect the components was typically <1/16 in. to avoid lateral mixing.

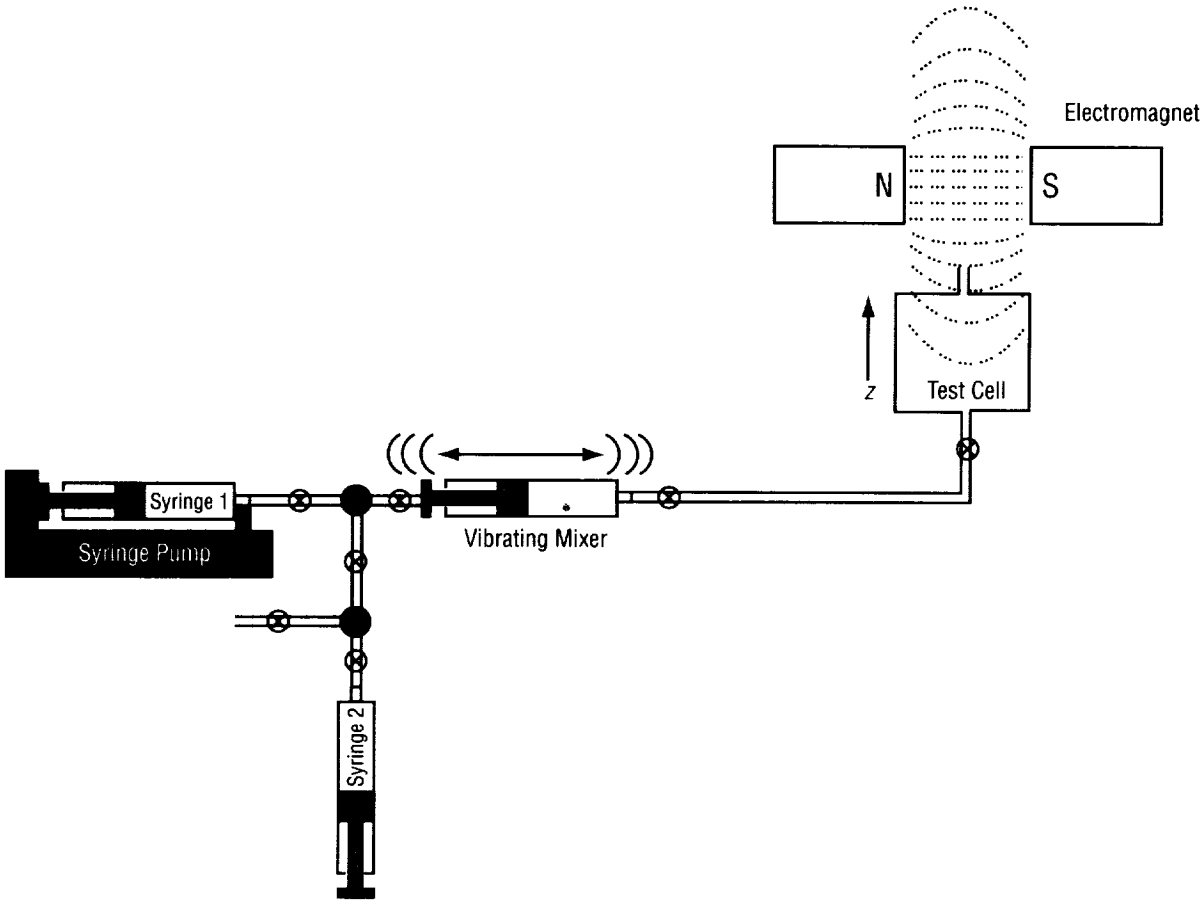

Figure 3. Arrangement of the experiment apparatus.

It can be shown (see app. B) that the vertical distribution of concentration C in the test cell is given by

$$C(z) = C_r + (C_{mo} - C_r)\exp\left(\frac{abz - v_{final}}{V_m}\right), \tag{9}$$

where C_r is the concentration in the supply syringe, C_{mo} is the initial concentration in the mixer, v_m is the volume of the mixer, and v_{final} is the final volume of fluid in the test cell with width a and depth b. Values of these parameters were selected to establish a clearly defined gradient as the supply syringe infuses the mixture into the test cell. As can be seen from eq. (9), the concentration (and thus the density) of the fluid entering the test cell from the bottom decreases during the deployment. In the absence of a magnetic field, this would be an unstable stratification and the denser fluid would sink to the bottom of the cell. However, with the magnet energized sufficiently, the lighter fluid simply displaces the denser fluid toward the top of the cell in the direction of the magnetic gradient.

4. PHOTOMETRIC ANALYSIS

This section describes a technique for measuring the fluid concentration in a test cell using photometric techniques. The work was guided by the efforts of Mihailovic and Beckermann[21] who used an argon ion laser as a monochromatic source and a 12-bit digital camera. The present effort uses a white backlight and optical filters to select the appropriate wavelengths. This allows for a greater selection of wavelengths to be tested to determine the optimum color for light attenuation through a particular fluid. In addition, the speckled nature of laser light, which may be non-uniform on small scales, can present a problem. However, their use of a 12-bit digital monochrome camera over our 10-bit camera is advantageous because the former generally has a superior dynamic range. Of course, the 12-bit camera requires much more computer memory for storing and manipulating the images. In either case, it is important that the camera provide a linear relation between light intensity and the associated pixel value.

It is often assumed that a CCD camera can be used as a kind of light meter in that the pixel values obtained by digitizing the analog signal out from the camera is proportional to the light intensity. A quick experiment was used to determine how well this holds. An image was captured containing two uniform targets, say 1 and 2, and their average gray level measured as A_1 and A_2, respectively. Next, the image brightness was adjusted by either changing the intensity of the incident light upon the targets, adjusting the gain of the camera, adjusting the f/stop of the camera lens, or placing a neutral density filter in front of the camera (this is the least acceptable as filters are not spatially uniform and often have a variability of a few percent). The image of the two targets was captured again and their average gray level measured as B_1 and B_2. For a "linear" camera, both images should get brighter or darker by the same percent, i.e.,

$$\frac{A_1}{A_2} = \frac{B_1}{B_2} \quad .$$

The above experiment was performed using a Sony® XC–7500 CCD camera and the results showed about a 6-percent difference between the two ratios. It was clear that the gray levels of the two targets did not change by the same proportion. Consequently, the camera is exhibiting a departure from linearity between image brightness and the resulting pixel value. A technique used to calibrate the nonlinear camera was developed with Soyoung Cha of the University of Illinois during his participation in the Marshall Space Flight Center Summer Faculty Program. A description of this method is beyond the scope of this paper, but will be published separately. After the camera was calibrated, the intensity ratios where within a percent of each other.

To measure the concentration distribution from the imagery, Beer's law is utilized which relates the two. Consider in fig. 4, a ray of light passing through a test cell filled with the ferrofluid. Ignoring refraction as well as scattering into and out of the beam, the initial (non-uniform) intensity $I_o(x,z)$ passes through a transparent wall of the test cell of thickness d and arrives at A with intensity

$$I_A(x,z) = I_o(x,z)\, e^{-\alpha_1(x,z)d} \quad ,$$

where $\alpha_1(x,z)$ is the attenuation coefficient varying spatially due to a non-uniform cell wall. After the ray passes through the ferrofluid of thickness s with varying concentration $C(z)$, it is further attenuated and arrives at B with intensity

$$I_B(x,z) = I_A(x,z)\, e^{-\alpha_\lambda sC(z)} = I_o(x,z) e^{-\alpha_1(x,z)d}\, e^{-\alpha_\lambda sC(z)} ,$$

where α_λ is the attenuation coefficient of the ferrofluid. Finally, the ray reaches D after passing through another wall of the test cell with intensity:

$$I_D(x,z) = I_B(x,z)\, e^{-\alpha_2(x,z)d} = I_o(x,z)\, e^{-d[\alpha_1(x,z)+\alpha_2(x,z)]}\, e^{-\alpha_\lambda sC(z)} , \tag{10}$$

where $\alpha_2(x,z)$ is the spatially-varying attenuation coefficient of the second wall of the test cell. Now let

$$Q(x,z) \equiv I_o(x,z)\, e^{-d[\alpha_1(x,z)+\alpha_2(x,z)]} ,$$

which contains the spatial variability of both I_o and that of the glass container. Thus eq. (10) becomes

$$I_D(x,z) = Q(x,z)\, e^{-\alpha_\lambda sC(z)} ,$$

or let the extinction coefficient be $\alpha = s\alpha_\lambda$ then

$$I_D(x,z) = Q(x,z) e^{-\alpha C(z)} . \tag{11}$$

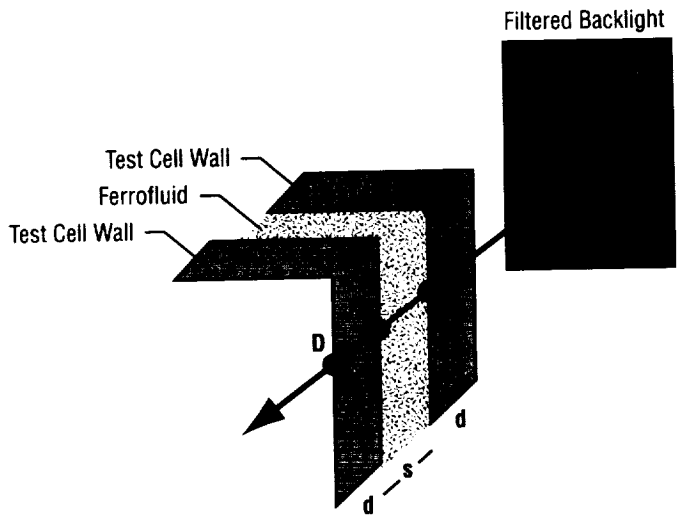

Figure 4. Schematic for development of the absorption equation.

To apply eq. (11) for retrieving the concentration, a vial of zero concentration (mineral oil only) was first placed in front of the filtered backlight and the two-dimensional image of the cell was digitized. This array is equivalent to $Q(x,z)$ which is now known from eq. (11) using C=0. Next, a vial with a known, constant fluid concentration C_K was placed in front of the filtered backlight at the same location. This two-dimensional image was digitized and stored as, say $I_D^K(x,z)$. Then the extinction coefficient was calculated from eq. (11) as

$$\alpha = \frac{1}{C_K} \ln \frac{Q(x,z)}{I_D^K(x,z)} \quad . \tag{12}$$

since everything on the right hand side is known. Averaging the fields $Q(x,z)$ and $I_D^K\left(x,z\right)$ before the division or simply averaging the quotient yielded essentially the same value for α. Finally, the concentration in any vial can now be determined by digitizing its image $[I_D(x,z)]$ and computing the concentration from eq. (11) as

$$C(z) = \frac{1}{\alpha} \ln \frac{Q(x,z)}{I_D(x,z)} \quad . \tag{13}$$

It should be noted that Beer's law applies at any specific wavelength and the absorption coefficient depends upon the selected frequency. For selecting the best filter used in front of the backlight, it is important that a wavelength be selected which allows the absorption coefficient to be constant and independent of concentration. A spectrophotometer was used to measure the absorption of known concentrations of test solution. Six different concentrations of the test solution were prepared in cells by diluting it with additional mineral oil, i.e., 0.75, 0.50, 0.40, 0.25, 0.15, and 0.05 ml/ml. Each sample was placed in a Coleman 44 Linear Absorbance Spectrophotometer, which measured the attenuation of light at selected wavelengths of 650, 635, 600, 520, and 440 nm. Suspecting that reflection of the incident light from the test cell could be an important factor in the transmittance of light, additional spectrophotometer measurements were made of a sample of the mineral oil and compared with that of air only. These data showed that the transmittance of light through the carrier liquid was higher than for air, not because there was less absorption in the liquid, but because there was less reflection of the incident light than for the container of air. By measuring the light attenuation, the extinction coefficient was computed in an effort to determine a particular wavelength where it might decouple from the concentration. A plot of the spectrophotometer measurements is shown in fig. 5.

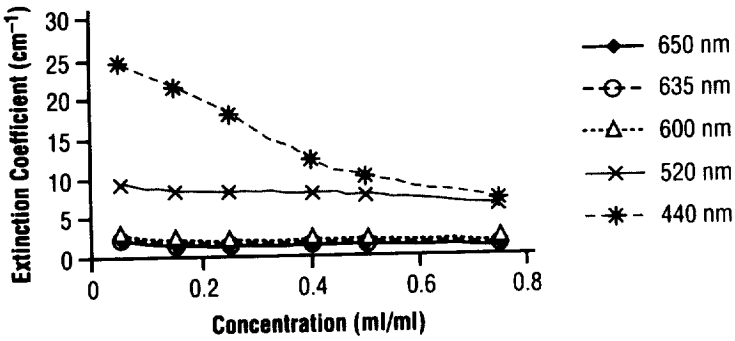

Figure 5. The extinction coefficient versus concentration measured at several wavelengths using a spectrophotometer.

It is clear that the extinction coefficient is fairly independent of concentration for the longer wavelengths so that red and green light would be candidates to use for photometrically measuring the concentration. From eq. (13), it can be seen that the relative error in concentration is proportional to the relative error in the extinction coefficient

$$\frac{\delta C}{C} = -\frac{\delta \alpha}{\alpha} \quad .$$

Thus from fig. 5, the best extinction coefficient is the one that is independent of concentration with the largest value (α) and the smallest variability ($\delta\alpha$).

The next step is to determine which bandpass filter should be used for our particular setup and compute the resulting extinction coefficient. Known concentrations of ferrofluid were prepared using a laboratory dispenser and are shown in table 1.

Table 1. Prepared (known) concentrations.

Vial No.	Amount of Ferrofluid (ml)	Amount of Carrier (ml)	Concentration
0	0.0	3.5	0.0
1	1.0	2.5	0.2857
2	0.9	2.6	0.2571
3	0.7	2.8	0.2
4	0.6	3.0	0.1667
5	0.5	3.0	0.1429
6	0.25	3.25	0.0714

With the white light passing through the vials, two green filters were separately placed in front of the camera. The first was a broad-spectrum Kodak No. 58 green filter with peak transmission around 520 nm. The other was a Melles Griot® 03FIL004 filter with transmission at 515 nm. Once the images were captured, the extinction coefficient was computed for each filter along with white light (no filter). Figure 6 shows a comparison of the calculated extinction coefficients. Clearly the Melles Griot filter is the best selection with an α value of 8.9. Using this extinction coefficient, the concentration was computed for each vial and compared with the known value. Figure 7 shows the two agree well.

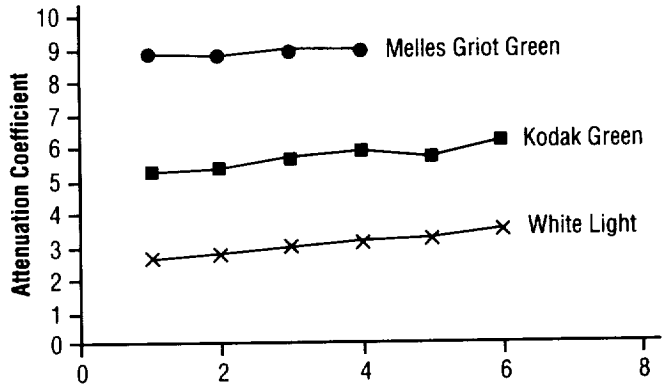

Figure 6. Calculation of the extinction coefficient for filtered and unfiltered light.

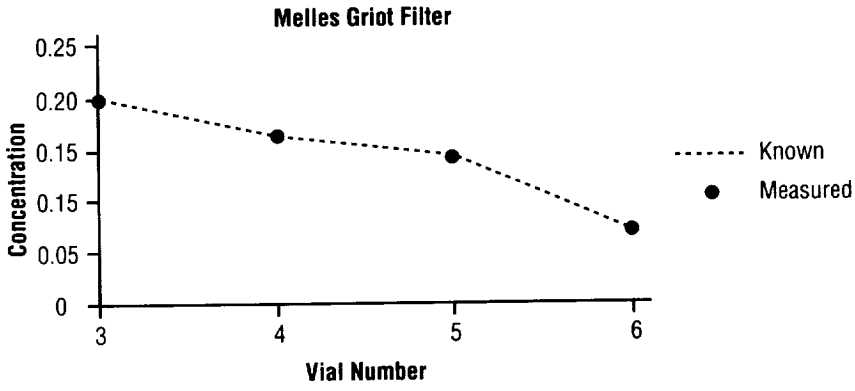

Figure 7. A comparison of the photometrically measured concentration versus the known (prepared) values.

One final consideration should be given to the design of the gradient experiment, i.e., the range of concentration expected. With an extinction coefficient for the Melles Griot filter at 8.9, the intensity curve was computed from eq. (11) and is shown in the fig. 8. Note that changes in concentration of the test solution ≈>0.4 have very little influence on the observed light intensity. Thus, this technique works best for low concentration values where changes result in large, measurable intensity changes.

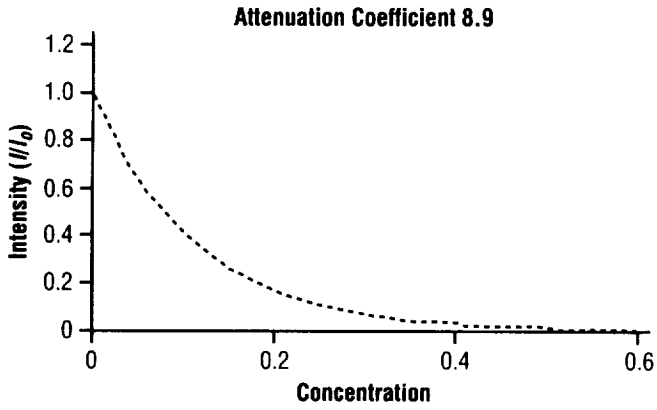

Figure 8. The theoretical reduction of intensity with increasing concentration.

With the experiment setup as in fig. 3, the mixer volume was set at 2.07 cc, the volume deployed was 3.68 cc, the initial concentration of the supply syringe was zero (i.e., mineral oil only), and the initial concentration of the mixer was 100-percent test solution. The supply syringe infused fluid into the mixer and forced fluid into the test cell. As the deployment continued, the test cell was injected from the bottom with fluid of decreasing concentration (and density) of ferrofluid. The fluid exhibited a slight jetting at the entrance of the test cell through the inlet needle. However, this effect is damped out as the deployment is completed and the experiment is allowed to equilibrate. The magnetic body force maintained this distribution throughout the experiment. The final distribution of fluid is shown in fig. 9 with the higher concentration in the upper regions. This configuration could be maintained indefinitely in the presence of the magnetic field. When the field was switched off, the fluid responded immediately by overturning to a stably-stratified distribution with the denser fluid on the bottom of the test cell. Interestingly, the original fluid gradient was recoverable in a rather short time by reapplying the magnetic field. The upper bound for this delay is dictated by the diffusion time scale, which is rather long in this case.

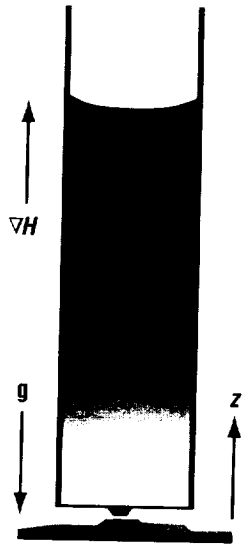

Figure 9. Test cell containing a concentration gradient stabilized by an overhead magnetic field.

For the experiment conditions above, the concentration profile was calculated from eq. (9) and is shown in fig. 10. The image of the test cell was digitized and analyzed to retrieve the concentration distribution. These measurements are also shown in fig.10 and agree well with the predicted values with an average error of 3 percent. Thus, the technique of using a magnetic field to deploy a prescribed concentration gradient has been demonstrated and quite suitable for a microgravity environment where small magnetic fields or fluids of lower magnetization could be employed. Although this technique for deploying a gradient is appropriate for a wide range of concentrations, measuring the distribution photometrically presents some difficulties. An appropriate wavelength to decouple the extinction coefficient from the concentration and the range of concentrations to produce a measurable change in intensity must be used. Other techniques for validating the concentration distribution include in situ measurements that extract samples from the test cell. The intrusive nature of this approach limits its application and would be disruptive in cases where the gradient is established as an initial condition for a separate experiment.

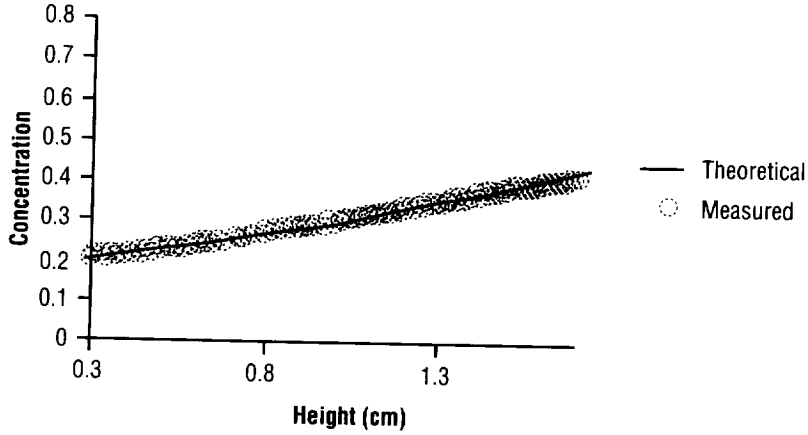

Figure 10. The measured and theoretical distribution of concentration in the test cell.

APPENDIX A—FERROFLUID DENSITY

For the theoretical analysis in this paper, it is necessary to know how the density of the ferrofluid changes with the volume fraction of solid magnetic particles. Equation (2) can be written as

$$\rho\beta = \frac{d\rho}{dC_v}\frac{dC_v}{d\phi} \quad , \tag{14}$$

where C_v is the volume concentration of the ferrofluid. For EMG 909 ferrofluid, pure (100 percent) ferrofluid contains a volume fraction of 3.6 percent so that

$$\frac{dC_v}{d\phi} = 27.8 \quad , \tag{15}$$

The variation of density with volume concentration was determined by preparing known concentrations of ferrofluid and then using a precision balance to measure the mass of a known volume. The first two rows of table 2 show the measured volumes of mineral oil and ferrofluid used. The measured mass of the mixture is shown in the fourth row and the computed density and concentration are shown in rows five and six.

Table 2. Fluid properties at various concentrations.

Property	Cell 1	Cell 2	Cell 3	Cell 4	Cell 5	Cell 6
Volume mineral oil (cc)	1.0	1.0	1.0	1.0	1.0	1.0
Volume ferrofluid (cc)	0.0	0.5	1.0	2.0	4.0	7.0
Total volume (cc)	1.0	1.5	2.0	3.0	5.0	8.0
Total mass (g)	0.697	1.128	1.568	2.544	4.427	7.198
Density (g/cc)	0.697	0.752	0.784	0.848	0.885	0.9
Concentration	0.0	0.333	0.5	0.667	0.8	0.875

A plot of the density as a function of volume concentration is shown in fig. 11 as well as a linear fit to the data. The slope of the line and thus $\frac{d\rho}{dC_v}$ is 0.242 g/cc. Consequently, eq. (14) can be estimated as $\rho\beta \approx 6{,}720$ kg/m^3.

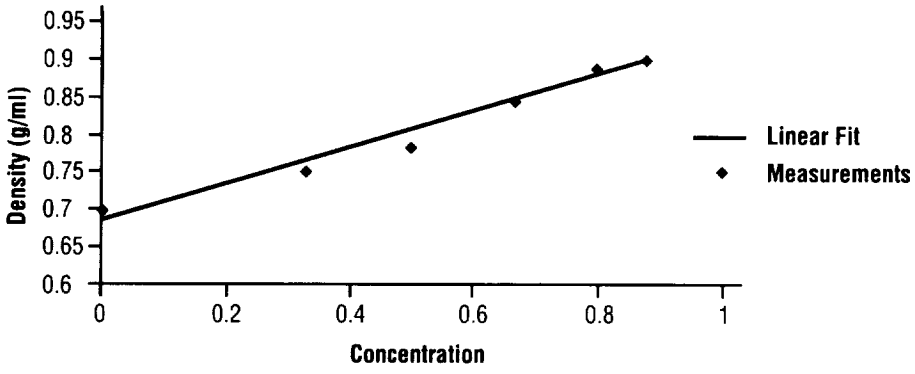

Figure 11. Variation of density with particle concentration.

APPENDIX B—CONCENTRATION GRADIENTS

B.1 General Case

Consider fig. 12 showing a reservoir of volume v_r containing fluid with a uniform concentration C_r and a mixer of volume v_m containing a different concentration C_m which varies in time. At the top of both containers are plungers, which can act independently to force fluid out of each container. Depression of the reservoir plunger forces its fluid into the mixer where it is rapidly mixed so that at any instant the concentration C_m is spatially uniform. Depression of the mixer plunger forces the mixed fluid out of the system.

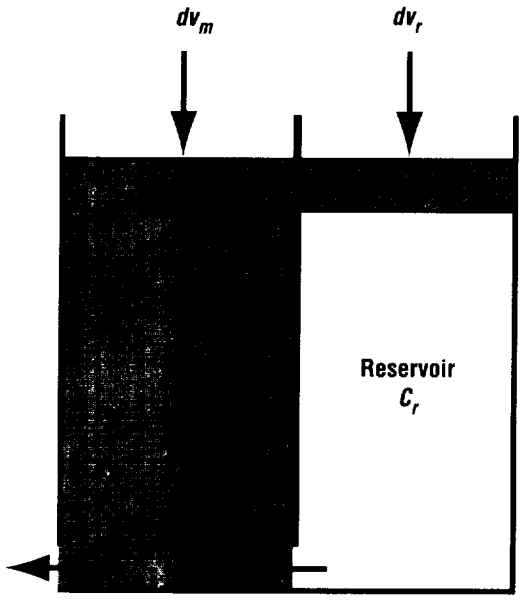

Figure 12. Gradient former.

Let n be the number of particles in the mixer and thus the concentration is

$$C_m = \frac{n}{v_m}$$

and

$$dn = v_m dC_m + C_m dv_m \ . \tag{16}$$

The number of particles flowing into the mixer from the reservoir is $-C_r dv_r$ and the number of particles flowing out of the mixer is $-C_m(dv_m+dv_r)$. Thus, eq. (16) becomes

$$-C_r dv_r + C_m(dv_m + dv_r) = v_m dC_m + C_m dv_m$$

or

$$\frac{dv_r}{v_m} = \frac{dC_m}{(C_m - C_r)} \quad . \tag{17}$$

Note that there is no change in the concentration of the mixer if either the volume of the reservoir is constant, the mixer volume is very large, or if the concentration in the reservoir is the same as that in the mixer.

B.2 Linear Gradient

If the two plungers are mechanically linked so that they move together, then $dv_r=dv_m$ and eq. (17) becomes

$$\frac{dv_m}{v_m} = \frac{dC_m}{(C_m - C_r)} \quad . \tag{18}$$

Integrating eq. (18) from the initial volume of the mixer v_{mo} at an initial concentration of C_{mo} to an arbitrary volume and concentration gives

$$\int_{v_{mo}}^{v_m} \frac{dv_m}{v_m} = \int_{C_{mo}}^{C_m} \frac{dC_m}{(C_m - C_r)}$$

or

$$C_m = C_r + (C_{mo} - C_r)\frac{v_m}{v_{mo}} \quad . \tag{19}$$

The total volume deployed out of the mixer v_t at any given time is $2(v_{mo}-v_m)$ so eq. (19) can also be written as

$$C_m = C_{mo} + (C_r - C_{mo})\frac{v_t}{2v_{mo}} \quad . \tag{20}$$

B.3 Exponential Gradient

If the plunger of the mixer is fixed so that v_m is a constant, then integrating the general eq. (17) from an initial reservoir volume v_{ro} when the mixer concentration is C_{mo} to an arbitrary volume and concentration yields

$$\frac{1}{v_m}\int_{v_{mo}}^{v_r} dv_r = \int_{C_{mo}}^{C_m} \frac{dC_m}{(C_m - C_r)}$$

or

$$C_m = C_r + (C_{mo} - C_r)\exp\left(\frac{v_r - v_{ro}}{v_m}\right) \quad . \tag{21}$$

The total volume deployed out of the mixer at any instant is $v_{ro}-v_r$ to that eq. (21) can also be written as

$$C_m = C_r + (C_{mo} - C_r)\exp\left(-\frac{v_t}{v_m}\right) \quad . \tag{22}$$

The unit of concentration used here is particles per total volume. A more convenient measure is volume concentration, which is the volume of test solution divided by the total volume of the mixture. This volume concentration then is also equivalent to the above concentration divided by the number of particles found in a unit volume of test solution. Since the two are related by a constant then both eq. (20) and eq. (22) are valid for volume concentration as well.

B.4 The Test Cell

It is often convenient to express the concentration as a function of height rather than volume deployed. Consider the test cell shown in fig. 13.

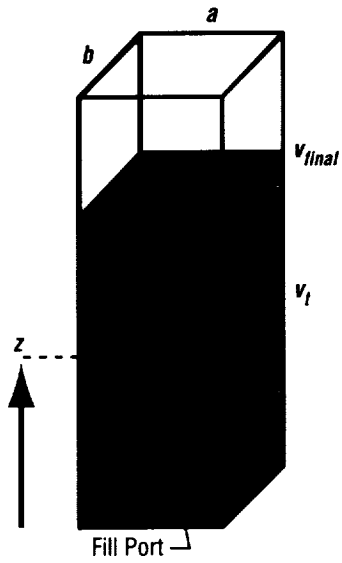

Figure 13. Test cell.

The origin of the z-axis is at the level of the fill port. At any z then, the volume deployed (i.e., the volume above z) is the final volume deployed into the test cell v_{final} minus the volume below z. For a test cell of width a and depth b, the volume deployed is

$$v_t(z) = v_{final} - abz \quad ,$$

so eq. (22) can be written as

$$C_m(z) = C_r + (C_{mo} - C_r)\exp\left(\frac{abz - v_{final}}{v_m}\right) \quad .$$

REFERENCES

1. Gillies, D.C.; Lehoczky, S.L.; Szofran, F.R.; Watring, D.A.; Alexander, H.A.; and Jerman, G.A.: "Directional Solidification of Mercury Cadmium Tellurium During the Second Microgravity Payload Mission (USMP–2)," in Space Processing of Materials, N. Ramachandran (ed.), SPIE 2809, pp. 2–11, 1996.

2. Odenbach, S.: "Convection Driven by Forced Diffusion in Magnetic Fluids," Phys. Fluids, Vol. 6, pp. 2535–2539, 1994.

3. Neuringer, J.L.; and Rosensweig, R.E.: "Ferrohydrodynamics," Phys. Fluids, Vol. 7, no. 12, p. 1927, 1964.

4. Zelazo, R.E.; and Melcher, J.R.: "Dynamics and Stability of Ferrofluids: Surface Interactions," J. Fluid Mech., Vol. 39, p. 1, 1969.

5. Finlayson, B.A.: "Convective Instability of Ferromagnetic Fluids," J. Fluid Mech., Vol. 40, p. 753, 1970.

6. Bashtovoi, V.G.; and Krakov, M.S.: "Stability of an Axisymmetric Jet of Magnetizable Fluid," translated from Z. Prik. Mekh. I Tekh. Fiz., No. 4, p. 147, July–August 1978.

7. Bashtovoi, V.G.: "Instability of a Motionless Thin Layer of a Magnetizable Liquid," translated from Z. Prik. Mekh. I Tekh. Fiz., No. 1, p. 81, January–February 1978.

8. Bashtovoi, V.G.: "Convective and Surface Instability of Magnetic Fluids," *Thermomechanics of Magnetic Fluids*, B. Berkovsky (ed.), Hemisphere Publishing Corporation, New York, NY, pp. 159–179, 1978.

9. Schwab, L.; Hilderbrandt, U.; and Stierstadt, K.: "Magnetic Bérnard Convection," J. Magnetism and Magnetic Matls., Vol. 38, pp. 113–114, 1983.

10. Stiles, P.J.; and Kagan, M.: "Thermo-Convective Instability of a Horizontal Layer of Ferrofluid in a Strong Vertical Magnetic Field," J. Magnetism and Magnetic Matls., Vol. 85, pp. 196–198, 1990.

11. Rosensweig, R.E.; Popplewell, J.; and Johnston, R.J.: "Magnetic Fluid Motion in a Rotating Field," J. Magnetism and Magnetic Matls., Vol. 85, p. 171, 1990.

12. Nakatsuka, K.; Hama, Y.; and Takahashi, J.: "Heat Transfer in Temperature-Sensitive Magnetic Fluids," J. Magnetism and Magnetic Matls., Vol. 85, pp. 207–209, 1990.

13. Aihara, T.; Kim, J-K.; Okuyama, K.; and Lasek, A.: "Controllability of Convective Heat Transfer of Magnetic Fluid in a Circular Tube," J. Magnetism and Magnetic Matls., Vol. 122, pp. 297–300, 1993.

14. Zebib, A.: "Thermal Convection in a Magnetic Fluid," J. Fluid Mech., Vol. 321, pp. 121–136, 1996.

15. Berkovsky, B.M.; and Smirnov, N.N.: "Capillary Hydrodynamic Effects in High Magnetic Fields," J. Fluid Mech., Vol. 187, p. 319, 1978.

16. Hörsten, W.V.; Odenbach, S.; and Stierstadt, K.: "Magnetic Bénard Convection Under Microgravity," Adv. Space Res., Vol. 11, pp. 251–254, 1991.

17. Odenbach, S.: "Drop Tower Experiments on Thermomagnetic Convection," Microgravity Sci. Technol., Vol. 6(3), pp. 161–163, 1993.

18. Odenbach, S.: "Sounding Rocket and Drop Tower Experiments on Thermomagnetic Convection in Magnetic Fluids," Adv. Space Res., Vol. 16, pp. 99–104, 1995.

19. Rosensweig, R.E.: *Ferrohydrodynamics*, Cambridge University Press, NewYork, NY, 1985.

20. Turner, J.S.: *Buoyancy Effect In Fluids*, Cambridge University Press, New York, NY, 1973.

21. Mihailovic, J.; and Beckermann, C.: "Development of a Two-Dimensional Liquid Species Concentration Measurement Technique Based on Absorptiometry," Exp. Thermal and Fluid Sci.; Vol. 10, pp. 113–123, 1995.

REPORT DOCUMENTATION PAGE

Form Approved
OMB No. 0704-0188

1. AGENCY USE ONLY *(Leave Blank)*	2. REPORT DATE	3. REPORT TYPE AND DATES COVERED
	July 2000	Technical Publication

4. TITLE AND SUBTITLE

The Use of Ferrofluids to Model Materials Processing
(MSFC Center Director's Discretionary Fund Final Report, Project No. 98–12)

5. FUNDING NUMBERS

6. AUTHORS

F. Leslie and N. Ramachandran*

7. PERFORMING ORGANIZATION NAMES(S) AND ADDRESS(ES)

George C. Marshall Space Flight Center
Marshall Space Flight Center, AL 35812

8. PERFORMING ORGANIZATION REPORT NUMBER

M–985

9. SPONSORING/MONITORING AGENCY NAME(S) AND ADDRESS(ES)

National Aeronautics and Space Administration
Washington, DC 20546–0001

10. SPONSORING/MONITORING AGENCY REPORT NUMBER

NASA/TP—2000–210386

11. SUPPLEMENTARY NOTES

Prepared by Microgravity Science and Applications Department, Science Directorate
*Universities Space Research Association, Huntsville, AL

12a. DISTRIBUTION/AVAILABILITY STATEMENT

Unclassified–Unlimited
Subject Category 34
Nonstandard Distribution

12b. DISTRIBUTION CODE

13. ABSTRACT *(Maximum 200 words)*

Many crystals grown in space have structural flaws believed to result from convective motions during the growth phase. The character of these instabilities is not well understood but is associated with thermal and solutal density variations near the solidification interface in the presence of residual gravity and g-jitter. To study these instabilities in a separate, controlled space experiment, a concentration gradient would first have to be artificially established in a timely manner as an initial condition. This is generally difficult to accomplish in a microgravity environment because the momentum of the fluid injected into a test cell tends to swirl around and mix in the absence of a restoring force. The use of magnetic fields to control the motion and position of liquids has received recent, growing interest. The possibility of using the force exerted by a non-uniform magnetic field on a ferrofluid to not only achieve fluid manipulation but also to actively control fluid motion makes it an attractive candidate for space applications. This paper describes a technique for quickly establishing a linear or exponential fluid concentration gradient using a magnetic field in place of gravity to stabilize the deployment. Also discussed is a photometric technique for measuring the concentration profile using light attenuation. Although any range of concentrations can be realized, photometric constraints impose some limitations on measurements. Results of the ground-based experiments indicate that the species distribution is within 3 percent of the predicted value.

14. SUBJECT TERMS	15. NUMBER OF PAGES
microgravity fluid dynamics, magnetic fluids	36
	16. PRICE CODE: A03

17. SECURITY CLASSIFICATION OF REPORT	18. SECURITY CLASSIFICATION OF THIS PAGE	19. SECURITY CLASSIFICATION OF ABSTRACT	20. LIMITATION OF ABSTRACT
Unclassified	Unclassified	Unclassified	Unlimited